DETC2019-97445

FEASIBILITY STUDY OF A CAPACITIVE MEMS FILTER USING ELECTROSTATIC LEVITATION

Mark Pallay

Mechanical Engineering Department Binghamton University Binghamton, New York, 13902 mpallay1@binghamton.edu

Shahrzad Towfighian *

Mechanical Engineering Department Binghamton University Binghamton, New York, 13902 stowfigh@binghamton.edu

ABSTRACT

We introduce a capacitive MEMS filter that uses electrostatic levitation for actuation and sensing. The advantage of this electrode configuration is that it does not suffer from the pullin instability and therefore tremendously high voltages can be applied to this system. A large sensing voltage will produce a large output signal, which boosts the signal to noise ratio. The filter outputs about a 110mV peak-to-peak signal when operated at 175V, and can be boosted to 175mV by increasing the voltage to 250V. Because pull-in is eliminated, voltages much higher than 250V can be applied. An outline of the filter design and operating principle is discussed. A model of the filter is derived and analyzed to show the mechanical response and approximate peak-to-peak signal output. This study shows the feasibility of a capacitive sensor that is based on electrostatic levitation, and outlines the advantages it has over traditional parallel-plate electrode configurations. This design is promising for signal signal processing applications where large strokes are important.

1 INTRODUCTION

Filtering is one of the most important and widely used techniques in signal processing. Many signals in everyday life are buried in noise and consist of many frequency components that must be filtered out to analyze the underlying electrical or mechanical signal. Like many signal processing procedures, filter-

ing is often performed by a data processing program on a computer, but in many cases it is impractical to computationally perform filtering because of cost, size, and energy requirements. For applications such as wireless transmitters and receivers, it is beneficial to perform filtering using electrical or mechanical phenomena that occur naturally and do not require a processor or computer. While simple high-pass, low-pass, and band-pass filters can be constructed using LRC circuits, mechanical filters that exploit resonance of a structure have a number of advantages over their purely electrical counterparts such as low power, significantly reduced size, and low cost per unit.

Since the early 1990s, capacitive MEMS filters have been developed to obtain large quality factors and high frequency tunability [1–7]. One common trait that exists for all of these filters is their electrode configurations are analogous to a parallel-plate capacitor. This is desirable because it can produce a large capacitiance that can be sensed easily, and the underlying dynamics of the electrostatic force are well understood. However, with all structures that have this type of electrode configuration, the system can become unstable when large voltages are applied and initiate pull-in. Pull-in failure is often permanent because of adhesion, which becomes more significant at small scales and can lead to stiction. Large voltages are desirable in capacitive sensors because they create high output signals that increase the signal-to-noise ratio.

One alternative to the parallel-plate electrode configuration is to use electrostatic levitation [8–13]. This method of actuation

^{*}Address all correspondence to this author.

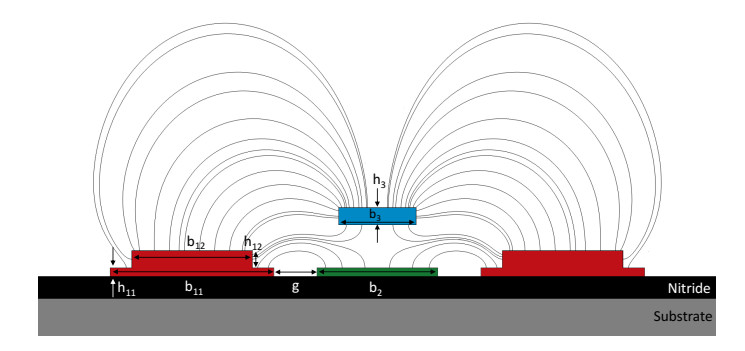


FIGURE 1. Repulsive force electrode configuration with cantilever beam (blue), fixed center electrode (green), and fixed side electrodes (red). The electrodes are deposited on $0.5\mu m$ of silicon nitride to insulate them from the bulk silicon.

adds an extra pair of electrodes on either side of the parallelplate structure to pull the two electrodes away from each other instead of together. A cross section of a beam undergoing electrostatic levitation is pictured in Figure 1. In this configuration, the side electrodes are charged and the center electrode and beam are grounded. The electric field from the side electrodes wraps around and pulls on the top of the beam more than the bottom, and the net force is upward. If the aspect ratio of the beams crosssection is large enough that the beam will only move up or down, pull-in will not occur because the center electrode is at the same voltage as the beam. This allows very large voltages to be applied to the system without creating instability or failure. The authors have previously applied 195V to the side electrodes without failure [11] and have the potential to go much higher with a slightly different fabrication procedure. Because electrostatic levitation eliminates pull-in, a capacitive sensor that is based on this design has no limit to the applied voltage and consequently no limit the the output voltage the sensor can produce.

In this paper, a MEMS filter that uses electrostatic levitation is introduced. The proposed filter does not experience pull-in and can be supplied with hundreds of volts to boost the signalto-noise ratio. This design is not limited by the trade off between maximum voltage and capacitance, which hinders the performance of current MEMS filters that are based on a parallelplate electrode configuration. The contribution of this study is to demonstrate the feasibility of a new filter design that uses a levitation-based capacitive sensor. These filters can theoretically produce large amounts of signal because of the high voltages that can be applied to them. The design of the filter and sensing circuit are outlined, and a cantilever model based on Hamilton's method is derived. The electrostatic force and associated capacitance is calculated with a finite-element model in COMSOL. The frequency response of the model is calculated to give a rough estimate of the output the device can achieve.

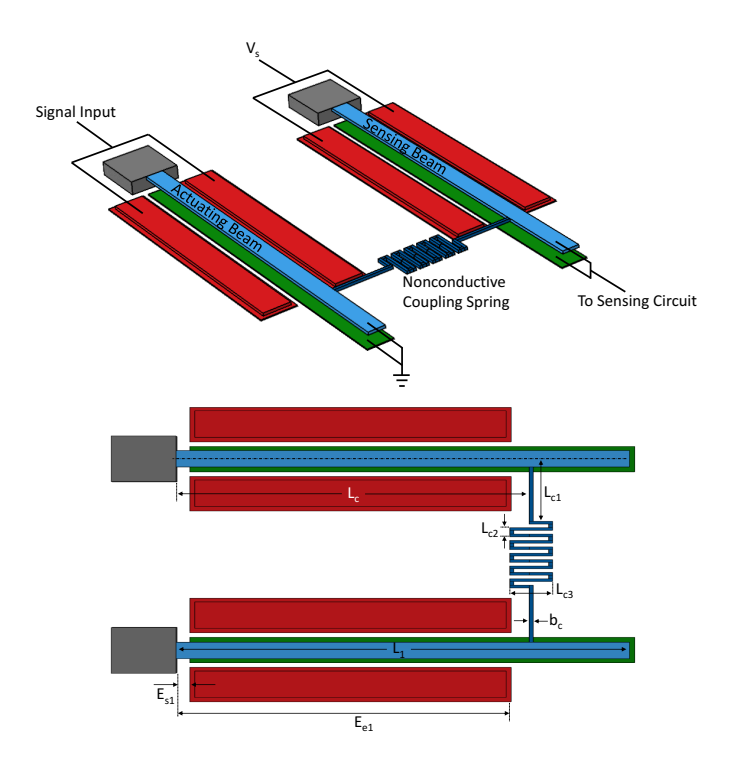


FIGURE 2. Layout of the filter

2 FILTER DESIGN

The design of the filter is shown in Figure 2 with dimensions given in Table 1. The filter is comprised of two polysilicon cantilever beams coupled with a serpentine spring. Each beam has has an electrostatic levitation electrode configuration with an extra layer of polysilicon on the side electrodes to increase the force and capacitance of the actuator and sensor respectively. Because the first two natural frequencies of the system are relatively low (15kHz and 30kHz), the system is designed to use the third and fourth natural frequencies, which correspond to the second symmetric and asymmetric modes of the system (103kHz and 105kHz).

Symmetric modes are when the two beams have the same shape and are traveling in the same direction, whereas asymmetric modes have the same shape but travel in the opposite direction. Because filters benefit from having symmetric and asymmetric natural frequencies close to each other, a thin serpentine coupling spring with five turns is used. It is also placed near the node of the second modes, which ensures that it does not bend significantly for the second asymmetric mode and does not add much stiffness to the system that would push the natural frequencies apart.

The side electrodes run from the anchor to the coupling spring. It has been demonstrated previously that partial electrodes can enhance the resonance of specific modes [14], and therefore the electrode length is chosen to boost the amplitude of

TABLE 1. Filter geometry and material properties

	~	
Parameter	Symbol	Value
Cantilever Length	L_1	$350\mu\mathrm{m}$
Beam Width	b_3	$18\mu\mathrm{m}$
Beam Thickness	h_3	$1.5 \mu m$
Initial Gap	d	$2\mu m$
Side Electrode Lateral Distance	g	5μm
Center Electrode Width	b_2	$28\mu\mathrm{m}$
Side Electrode Layer 1 Width	b_{11}	$38\mu m$
Side Electrode Layer 2 Width	b_{12}	$28\mu m$
Side Electrode Start	E_{si}	$10\mu\mathrm{m}$
Side Electrode End	E_{ei}	$263 \mu m$
Electrode Layer 1 Thickness (µm)	h_{11}	$0.5 \mu \mathrm{m}$
Electrode Layer 2 Thickness (µm)	h_{12}	$2\mu m$
Elastic Modulus	E	160GPa
Density	ρ	$2330 \ ^{kg}/m^3$
Poisson's Ratio	v	0.22
Coupling Spring Location	L_c	$274.2\mu\mathrm{m}$
Coupling Spring Width	b_c	$3\mu m$
Coupling Spring Length 1	L_{c1}	$70 \mu \mathrm{m}$
Coupling Spring Length 2	L_{c2}	$7\mu\mathrm{m}$
Coupling Spring Length 3	L_{c3}	$30\mu m$
Number of Spring Turns	n	5

the second symmetric and asymmetric modes. On the actuating beam, the side electrodes are supplied with the pre-filtered signal superimposed on a high DC voltage. The actuating beam and center electrode are grounded to induce electrostatic levitation. The coupling spring is assumed to be nonconductive so that the beams can remain electrically isolated while being mechanically connected to each other. On the sensing beam, the side electrodes are given the same DC voltage as the actuating electrode, however, the beam and center electrode are connected and fed into a capacitive sensing circuit. It is important to have the same DC offset for both the sensor and actuator to ensure the natural frequencies stay close together since the levitation force creates a stiffening effect on the beams. As the signal is fed into the actuator, the actuating beam moves in response to the changing volt-

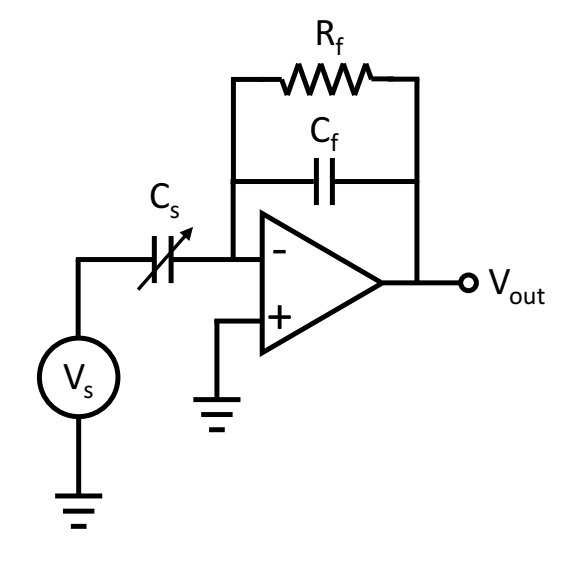


FIGURE 3. Sensing circuit of the filter

age. This motion is transferred to the sensing beam through the coupling spring, and the capacitance between the beam/center electrode and side electrodes is sensed.

The sensing circuit is pictured in Figure 3 and consists of an op-amp, a resistor, and a capacitor. The voltage source (V_s) and sensor capacitor (C_s) are the applied voltage and capacitance of the sensing beam as pictured in Figure 1. The other capacitor (C_f) , resistor (R_f) , and op-amp act as a charge amplifier. If R_f is sufficiently large, the output of the sensing circuit can be estimated by the relationship,

$$V_{out} = \frac{C_s V_s}{C_f} \tag{1}$$

Equation (1) scales linearly with the applied voltage to the sensor. Because electrostatic levitation is inherently stable and will not create pull-in, V_s can be increased significantly to boost the amount of output signal of the filter.

3 MODEL DERIVATION

A model of the filter is derived with Hamilton's principle, shown in Equation (2).

$$\int_{t_1}^{t_2} \left[\delta T - \delta V + \delta W_{nc} \right] dt = 0 \tag{2}$$

where δT is the variational kinetic energy, δV is the variational potential energy, and δW_{NC} is the virtual work of nonconservative forces, such as damping. The coupling spring is assumed to have negligible mass and therefore will not significantly affect the inertia and kinetic energy of the system. However, its stiffness is not negligible and will have an associated strain energy

that will appear in the variational potential energy term. The kinetic energy, potential energy, and virtual work are shown in the equations below,

$$T_{beam} = \frac{1}{2} \int_{0}^{L} \left[\rho_{1} A_{1} \dot{w}^{2} H \left(L_{1} - x \right) + \rho_{2} A_{2} \dot{w}^{2} H \left(x - L_{1} \right) \right] dx \quad (3)$$

$$V_{beam} = \frac{1}{2} \int_{0}^{L} \left[E_{1} I_{1} w_{xx}^{2} H \left(L_{1} - x \right) + E_{2} I_{2} w_{xx}^{2} H \left(x - L_{1} \right) \right] dx \quad (4)$$

$$V_{elec} = \int_{E_{s1}}^{E_{e1}} \left[V_{s}^{2} \left(\int f_{e}(w) dw \right) H \left(L_{1} - x \right) + \right] dx + \int_{E_{s2}}^{E_{e2}} \left[V_{a}^{2} \left(\int f_{e}(w) dw \right) H \left(x - L_{1} \right) + \right] dx \quad (5)$$

$$V_{spring} = \frac{1}{2} k_{ct} \left(w(L_{c1}) - w(L_{c2}) \right)^{2} + \frac{1}{2} k_{cr} \left(w_{x}(L_{c1}) - w_{x}(L_{c2}) \right)^{2} \quad (6)$$

where T_{beam} and V_{beam} are the kinetic and bending strain energy of the beam respectively, V_{elec} is the potential energy from the electrostatic force (f_e) , V_{spring} is the potential energy of the coupling spring, δW_{nc} is the virtual work from damping, w is the transverse deflection of the beam, L is the total length of the x-domain, V_s and V_a are the side voltages on the sensor and actuator respectively, k_{ct} and k_{cr} are the transnational and rotational stiffness of the coupling spring, and H(x) is the Heaviside step function.

 $\delta W_{nc} = \int_{0}^{L} \left[c_1 \dot{w} \delta w H \left(L_1 - x \right) + c_2 \dot{w} \delta w H \left(x - L_1 \right) \right] dx$

The x-domain of the system runs along the length of both beams, starting at the anchor of beam 1 and ending at the free end of beam 2. There is a discontinuity between the free end of beam 1 and the fixed end of beam 2, however this is accounted for in the boundary conditions. There are 16 total boundary conditions derived from Equation (2), 8 of which are the standard boundary conditions for a cantilever beam (4 for each beam), and the other 8 specify continuous displacement and slope, a moment force balance, and shear force balance at the location of the coupling spring.

Solving for the variation of the energy terms in Equations (3)-(7) and plugging them into Equation (2), yields the governing equation of motion for the system shown in Equation (8).

$$(\rho_1 A_1 \ddot{w} + c_1 \dot{w} + E_1 I_1 w_{xxxx} - V_s^2 f_e(w)) H(x - L_1) + (\rho_2 A_2 \ddot{w} + c_2 \dot{w} + E_2 I_2 w_{xxxx} - V_a^2 f_e(w)) H(L_1 - x) = 0$$
 (8)

In Equation (8) there are two partial differential equations (PDE) that are separated by the Heaviside step function. These PDEs govern the motion of each beam as a function of the applied voltages. Because the two beams are assumed to be identical, the material properties and geometries both beams are the

same (e.g. $\rho_1 = \rho_2 = \rho$). It should be noted that the coupling spring does not show up in the governing equation because it is accounted for in the boundary conditions. The electrostatic force, f_e , is calculated in COMSOL and fit with a 5^{th} order polynomial.

The equation is nondimensionalized and Galerkin's method is performed to reduce the PDE into a set of coupled ordinary differential equations (ODEs) that can be solved numerically. The total deflection is separated into time dependent components, η_i and space dependent components (mode shapes), ϕ_i , with a four mode approximation, and the linear terms are decoupled by exploiting the orthogonality of the mode shapes. The mode shapes, which depend on the boundary conditions, are obtained numerically in COMSOL using the model shown in Figure 2 without considering the effect of the electrostatic force. The decomposition yields 4 ODEs coupled through their nonlinear terms:

$$\ddot{\eta}_{j} + c_{j}\dot{\eta}_{j} + \lambda_{j}^{4}\eta_{j} - \sum_{i=0}^{5} \alpha_{ij} \left(V_{s}^{2} \int_{E_{s1}}^{E_{e1}} \phi_{j} \left[\sum_{k=1}^{4} \phi_{k} \eta_{k} \right]^{i} dx + V_{a}^{2} \int_{E_{s2}}^{E_{e2}} \phi_{j} \left[\sum_{k=1}^{4} \phi_{k} \eta_{k} \right]^{i} dx \right) = 0 \quad (9)$$

where

$$\alpha_{ij} = \frac{L_1^4 \beta_i h_3^{i-1}}{E I m_j}$$
 $m_j = \int_0^1 \phi_j^2 dx$ $c_j = \frac{\lambda_j^2}{Q}$ (10)

For the analysis, the sensor voltage, V_s , is a constant DC voltage upwards of 100V. The actuator voltage is the input signal, which is a sinusoidal function superimposed on the same DC that is applied to the sensor. Equation (9) is integrated in MAT-LAB to find the time response of the system. This is repeated at many frequencies to obtain a frequency response around the 2nd symmetric and asymmetric natural frequencies of the filter.

4 RESULTS AND DISCUSSION

The frequency response of the filter around 100kHz at 175V is shown in Figure 4. A damping quality factor of 100 was chosen to simulate a relatively low pressure environment. Previous experiments by the authors have demonstrated this to be on the order of about 1 Torr for cantilevers with a similar design to the filter [11,12]. The sensor shows up to 5μ m of dynamic tip displacement about a static position of approximately 9μ m. The filter has a center frequency of 105kHz, a bandwidth of about 2.7kHz, and a pass-band ripple of 5.28dB.

The filter is suitable for low frequency applications. The bandwidth and pass-band ripple are larger than many other MEMS filters, though both can be improved by decreasing the damping. However, the focus of this study is not to design the optimal filter, but to demonstrate the feasibility and advantages

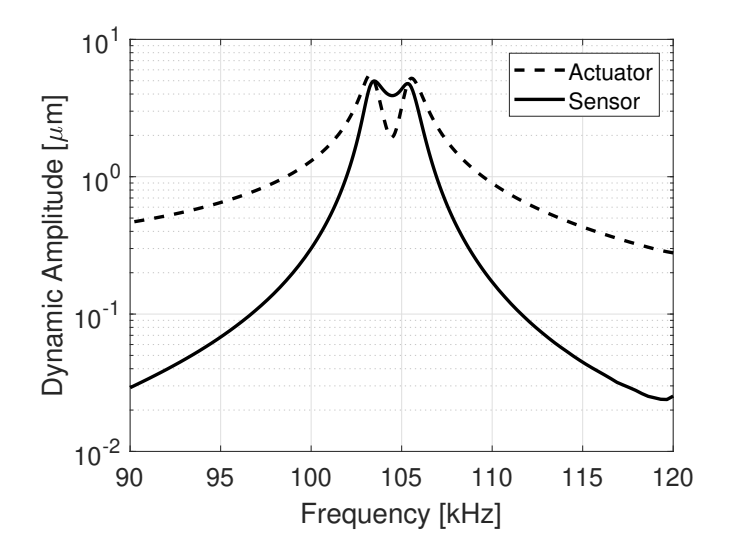


FIGURE 4. Frequency response at Q=100, $V_s = 175V$, $V_{aDC} = 175V$ and $V_{aAC} = 25V$. Displacement is calculated at the tip of each beam.

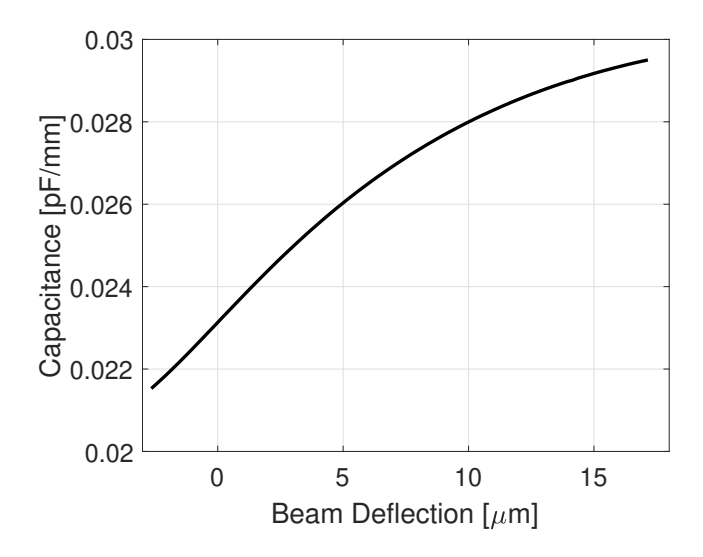


FIGURE 5. Capacitance per unit length as a function of beam displacement.

of the electrostatic levitation-based capacitive sensor. In this pursuit, the capacitance between center and side electrodes can be calculated in COMSOL. The beam and center electrode are wired together and treated as a single electrode. The same is done for the side electrodes. The capacitance per unit length is shown in Figure 5.

The capacitance of this structure is much smaller than a traditional parallel-plate structure. Figure 5 shows around 25

fF/mm, and a change of less than 10 fF/mm as the beam deflects over $15\mu m$. The total capacitance of the sensing beam can be estimated by calculating the capacitance per unit length at each point along the the deflected beam from the start to the end of the side electrodes. This can be integrated along the length with the deformed shape of the beam to find the total capacitance, which can be used in Equation (1) to estimate the voltage output.

The total capacitance was estimated at the minimum and maximum beam deflection at the peak frequency in Figure 4. At 103,480Hz, the maximum and minimum tip displacement is 13.3μ m and 4.56μ m including the static deflection. This correlates to a maximum and minimum capacitance of 6.5 fF and 5.9 fF. If C_f is chosen to be about a picofarad, this will produce an output voltage of 111.3mV peak-to-peak. Modifying the geometry of the filter, such as increasing the height of the side electrodes or adding fins to the beam can increase the capacitance and voltage output. This will result in more levitation force, and because pull-in is eliminated, this is not problematic.

The main advantage of this system is that even if the output signal is small, the sensing voltage can be increased without the risk of the sensor becoming unstable. To demonstrate this, the sensing voltage is increased to 250V and the frequency response is shown in Figure 6. In this case the dynamic deflection at the peak increases by about 1μ m and the total voltage output is boosted to 174.6mV. By increasing the applied voltage by 43%, the output signal was boosted by 57% and the dynamic response of the of the filter was not hindered. In fact, with a higher voltage the dynamic response of the sensors was improved and showed a larger dynamic deflection, which correlated to a larger change in capacitance. This shows a filter that uses an electrostatic levitation-based capacitive sensor can be supplied with very high sensing voltages to boost the output signal without creating instability or negatively affecting the dynamic response.

5 CONCLUSION

In this study, a novel MEMS filter that uses an electrostatic levitation-based capacitive sensor is introduced. This electrode configuration does not suffer from pull-in, and therefore very high voltages upwards of 200V can be applied. The theoretical signal output of the filter was boosted from 111.3mV to 174.6mV by increasing the sensor voltage from 175V to 250V. From a theoretical standpoint, this voltage could be increased even further to increase the output signal even more. Because the input signal is superimposed on the applied voltage, increasing the sensing voltage also increases the mechanical response of the filter, which further boosts its performance. The capacitance associated with electrostatic levitation is small, so high sensing voltages do not produce as much output signal as they would in a parallel-plate system. However, the design can be further optimized to increase the capacitance and potentially outperform the current generation of MEMS filters. This result is promising not

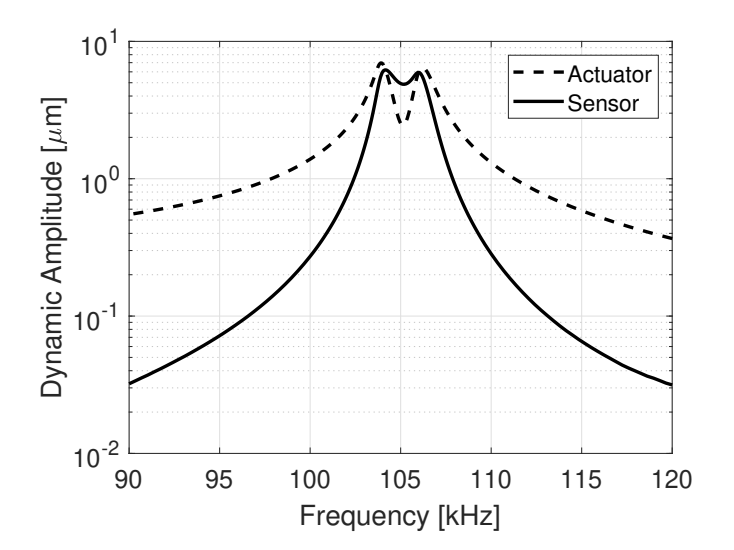


FIGURE 6. Frequency response at Q=100, $V_s = 250V$, $V_{aDC} = 250V$ and $V_{aAC} = 25V$. Displacement is calculated at the tip of each beam.

only for filters, but for any capacitive sensing device that would benefit from a high signal-to-noise ratio.

6 Acknowledgment

This research is funded by NSF grant ECCS #1608692.

REFERENCES

- [1] Nathanson, H. C., Newell, W. E., Wickstrom, R. A., and Davis, J. R., 1976. "The resonant gate transistor". *IEEE Transactions on Electron Devices*, *14*(3), pp. 117–133.
- [2] Lin, L., Howe, R. T., and Pisano, A. P., 1998. "Microelectromechanical filters for signal processing". *Journal of Microelectromechanical Systems*, 7(3), pp. 286–294.
- [3] Wang, K., and Nguyen, C. T.-C., 1999. "High-order medium frequency micromechanical electronic filters". *Journal of Microelectromechanical Systems*, 8(4), pp. 534–557.
- [4] Wong, A.-C., and Nguyen, C. T.-C., 2004. "Micromechanical mixer-filters ("mixlers")". *Journal of Microelectromechanical Systems*, *13*(1), pp. 100–112.
- [5] Motiee, M., Mansour, R. R., and Khajepour, A., 2006. "Novel mems filters for on-chip transceiver architecture, modeling and experiments". *Journal of Micromechanics and Microengineering*, 16(2), pp. 407–418.
- [6] Hajhashemi, M., Amini, A., and Bahreyni, B., 2012. "A micromechanical bandpass filter with adjustable bandwidth and bidirectional control of centre frequency". Sensors and Actuators A, 187, pp. 10–15.

- [7] Hafiz, M. A. A., Kosuru, L., Hajjaj, A. Z., and Younis, M. I., 2017. "Highly tunable narrow bandpass mems filter". *IEEE Transactions of Electron Devices*, 64(8), pp. 3392–3398.
- [8] Lee, K. B., and Cho, Y. H., 2001. "Laterally driven electrostatic repulsive-force microactuators using asymmetric field distribution". *Journal of Microelectromechanical Systems*, 10(1), pp. 128–136.
- [9] He, S., and Ben Mrad, R., 2005. "Large-stroke microelectrostatic actuators for vertical translation of micromirrors used in adaptive optics". *IEEE Transactions on Industrial Electronics*, *52*(4), pp. 974–983.
- [10] Fan, C., and He, S., 2015. "A Two-Row Interdigitating-Finger Repulsive-Torque Electrostatic Actuator and Its Application to Micromirror Vector Display". *Journal of Microelectromechanical Systems*, 24(6), pp. 2049–2061.
- [11] Pallay, M., Daeichin, M., and Towfighian, S., 2017. "Dynamic Behavior of an Electrostatic MEMS Resonator with Repulsive Actuation". *Nonlinear Dynamics*, 89(2), pp. 1525–1538.
- [12] Pallay, M., and Towfighian, S., 2018. "A parametric electrostatic resonator using repulsive force". *Sensors and Actuators A: Physical*, **277**, pp. 134 141.
- [13] Ozdogan, M., Daeichin, M., Ramini, A., and Towfighian, S., 2017. "Parametric Resonance of a Repulsive Force MEMS Electrostatic Mirror". Sensors and Actuators A Physical,, 265, pp. 20–31.
- [14] Nizar, J., Ramini, A., Carreno, A. A., and Younis, M. I., 2016. "Higher order modes excitation of electrostatically actuated clamped–clamped microbeams: experimental and analytical investigation". *Journal of Micromechanics and Microengineering*, 26(2), p. 025008.